# Azimuthal Anisotropy Scaling for Identified Mesons and Baryons: Insights into Medium Transport Properties, Equation of State and Hadronic Re-scattering

**Roy A. Lacey,**[*1]

[1] *Depts of Chemistry and Physics, Stony Brook University, Stony Brook, NY, 11794, USA*

## Abstract

Species-resolved azimuthal anisotropy scaling functions are constructed from measurements of $v_2(p_T, \text{cent})$ and $v_3(p_T, \text{cent})$ for identified mesons and baryons over a broad $p_T$ range in Pb+Pb ( $\sqrt{s_{NN}} = 2.76$ and 5.02 TeV) and Xe+Xe (5.44 TeV) collisions at the LHC, and in U+U, Au+Au, Cu+Au, and Cu+Cu collisions at top RHIC energy. The scaling functions exhibit robust data collapse across centralities and collision systems, extending from the low-$p_T$ collective regime into the high-$p_T$ quenching-dominated region. Simultaneous intra-harmonic scaling and inter-harmonic mapping separate geometric inputs from response coefficients associated with attenuation, radial flow, and late-stage hadronic re-scattering. The constrained coefficients exhibit distinct trends: $k_\beta$ varies primarily with beam energy and attenuation conditions, $\zeta_{\rm rf}$ evolves strongly with centrality and multiplicity while retaining additional system and beam-energy dependence, and $\zeta_{\rm hs}$ is negligible for the LHC cases studied but finite for the RHIC systems. These trends substantially restrict interchangeability among the response coefficients and provide complementary sensitivity to viscous attenuation, partonic energy loss, collective expansion, and hadronic dynamics. The evolution of $\zeta_{\rm rf}$ also provides sensitivity to the equation of state, while geometry-sensitive inter-harmonic scaling provides system-consistent constraints on intrinsic quadrupole deformation, yielding preferred values of $\beta_2 \approx 0.18$ for Xe and $\beta_2 \approx 0.20$ for U. These results establish species-resolved anisotropy scaling as a quantitative, data-driven framework for charting QGP response and nuclear geometry.

*Keywords:* Azimuthal anisotropy, Identified-particle anisotropy, Scaling functions, Quark–gluon plasma, Transport coefficients, Hadronic re-scattering

*DOI:* 10.31526/PHEP.2026.47

## 1. INTRODUCTION

High-energy heavy-ion collisions at the Large Hadron Collider (LHC) and Relativistic Heavy Ion Collider (RHIC) create the quark–gluon plasma (QGP), a state of matter that recreates conditions microseconds after the Big Bang [1, 2, 3]. Determining the QGP transport coefficients and equation of state (EOS) is essential for understanding its evolution and thermodynamic properties.

A primary probe of these properties is azimuthal anisotropy, which reflects the medium's response to initial spatial asymmetries. At low transverse momentum ($p_T$), anisotropies arise predominantly from collective flow, while at higher $p_T$ they encode path-length–dependent partonic energy loss (jet quenching). The anisotropy is quantified by the complex Fourier coefficients $V_n$ [4, 5, 6],

$$V_n \equiv v_n e^{in\Psi_n} = \langle e^{in\phi} \rangle, \tag{1}$$

where $v_n$ is the magnitude, $\Psi_n$ the symmetry-plane angle, and $\langle\cdot\rangle$ denotes an average over the single-particle azimuthal distribution.

Experimentally, the anisotropy coefficients are commonly extracted using the Scalar Product (SP) method [7, 8], which correlates the unit flow vector of a particle of interest with an event-wide flow vector constructed from reference particles,

$$\mathbf{u}_{n,k} = e^{in\varphi_k}, \qquad \mathbf{Q}_n = \sum_i w_i e^{in\varphi_i},$$

where $\varphi_k$ and $\varphi_i$ are the azimuthal angles of the particle of interest and reference particles, respectively, and $w_i$ accounts for detector acceptance and reconstruction efficiency. A pseudorapidity gap between the particle of interest and the reference sub-events suppresses non-flow correlations. The resulting anisotropy coefficients are given by

$$v_n\{\text{SP}\} = \frac{\left\langle \langle \mathbf{u}_{n,k} \mathbf{Q}_n^* \rangle \right\rangle}{\sqrt{\frac{\langle \mathbf{Q}_n \mathbf{Q}_n^{A*} \rangle \langle \mathbf{Q}_n \mathbf{Q}_n^{B*} \rangle}{\langle \mathbf{Q}_n^A \mathbf{Q}_n^{B*} \rangle}}}, \tag{2}$$

where the superscripts $A$ and $B$ denote independent reference sub-events used to correct for finite event-plane resolution. Single brackets $\langle\cdot\rangle$ indicate event averages, while double brackets $\langle\langle\cdot\rangle\rangle$ denote averages over particles within and across events. The denominator provides the standard SP resolution correction through correlations between the two reference sub-events.

Extensive experimental and theoretical studies [9, 10, 11, 12, 13, 14, 15, 16, 17, 18, 19, 20, 21, 22, 23, 24, 25, 26, 27, 28, 29, 30, 31, 32, 33, 34, 35] have established that the anisotropy coefficients $v_n(p_T, \text{cent})$ encode the coupled response of the medium to initial-state eccentricities $\varepsilon_n$ (and their fluctuations), viscous attenuation, radial flow, partonic energy loss, and hadronic re-scattering. Collective dynamics dominate for $p_T \lesssim 4$–5 GeV/$c$, while anisotropies at higher $p_T$ are governed primarily by jet quenching.

Recent work [36] introduced anisotropy scaling functions for charged hadrons, providing a unified description of $v_{2,3}(p_T, \text{cent})$ across broad $p_T$ and centrality ranges. These scaling relations explicitly incorporate the initial eccentricity spectrum that seeds the azimuthal anisotropy and constrain the viscous and quenching responses associated with the specific shear viscosity $\eta/s$ and the jet-quenching parameter $\hat{q}$. Charged-hadron measurements, however, average over many particle species, obscuring species-dependent effects associated with particle mass, baryon number, and hadronic cross section.

Species-resolved measurements restore this discriminatory power by exposing mass-, baryon-number–, and hadronic-coupling dependencies that are averaged out in inclusive observables. Within the scaling framework, these dependencies are not merely cataloged but

*Corresponding author: Roy.Lacey@Stonybrook.edu

are leveraged quantitatively: species-dependent blue shifts and attenuations are encoded directly in the scaling functions and their associated exponents. The initial eccentricities $\varepsilon_n$ specify the geometric response, while the common attenuation and species-dependent scaling parameters constrain the medium response to viscous attenuation, partonic energy loss, radial flow, and hadronic re-scattering. In particular, the mass- and baryon-number–dependent blue shift of the scaled distributions constrains the radial-flow response, whose systematic evolution with multiplicity and beam energy provides an empirical handle on EOS-driven pressure gradients. At higher $p_T$, controlled departures from perfect scaling constrain how partonic energy loss is transmitted through hadronization and baryon–meson systematics.

Additional leverage is obtained by exploiting differences in hadronic cross section. Within the scaling functions, hadrons with small cross sections (e.g., $K^{\pm}$, $\phi$, $\Xi^{\pm}$, $\Omega^{\pm}$) define an early-decoupling baseline that preserves partonic flow patterns and the radial-flow–induced blue shift. In contrast, large–cross-section species (e.g., $\pi^{\pm}$, $p$, $\bar{p}$) exhibit systematic, species-dependent suppression relative to this baseline. These deviations provide a quantitative constraint on the influence of late-stage hadronic re-scattering. Because such re-scattering occurs after the partonic phase, its species-dependent influence can be distinguished from the common geometric and early-time attenuation response, providing separate scaling constraints on radial-flow and hadronic-response contributions.

Earlier studies have explored event-by-event correlations between $\langle p_T \rangle$ and $v_n$ fluctuations as indirect probes of radial flow and viscous effects [37, 38]. While such correlations are sensitive to transverse pressure gradients, they inherently entangle multiple sources of fluctuations, including initial-state geometry, viscous attenuation, multiplicity fluctuations, and late-stage hadronic re-scattering. This convolution precludes a clean separation of geometric and transport effects and obscures the specific contribution of radial flow. By contrast, the species-resolved scaling framework developed here treats geometric inputs, viscous attenuation, radial flow, and hadronic re-scattering as distinct components of the scaling response, enabling data-driven constraints without reliance on fluctuation-induced correlations.

## 2. SPECIES-RESOLVED FRAMEWORK

In this work, the charged-hadron scaling methodology [36] is extended to identified mesons ($\pi^{\pm}$, $K^{\pm}$, $K^0_S$, $\phi$) and baryons ($p$, $d$, $^3$He, $\Lambda^0$, $\Xi^-$, $\Omega^-$), with the aim of constructing species-resolved scaling functions for $v_{2,3}(p_T, \text{cent})$. The formalism preserves the acoustic/hydrodynamic structure of the charged-hadron framework while incorporating explicit mass, baryon-number, and hadronic-coupling dependences, thereby enabling the species-dependent blue shift associated with radial flow and the attenuation from late-stage hadronic re-scattering to provide complementary constraints on the medium response. A key feature of the framework is that the same scaling structure is applied continuously across the measured $p_T$ range, connecting the low- and intermediate-$p_T$ collective regime to the high-$p_T$ quenching-dominated regime. The same framework is then applied across particle species, centralities, collision systems, and beam energies, providing multiple, complementary constraints on a common medium-response description.

A focused application of the present species-resolved framework to beam-energy-dependent baryon transport and baryon-junction-related phenomena was subsequently presented in Ref. [39]. While that work emphasized the interpretation of beam-energy-dependent transport trends associated with baryon transport, the present study is concerned with the broader development, validation, and interpretation of the species-resolved scaling framework itself, including its implications for viscous attenuation, radial flow, hadronic re-scattering, geometry-driven scaling behavior, and deformation-sensitive medium response across collision systems and particle species.

Species-resolved scaling is anchored to the kaon scaling function in ultra-central (uc, 0–1%) Pb+Pb collisions at $\sqrt{s_{NN}} = 5.02$ TeV, which serves as the universal reference [39]. Kaons provide an optimal baseline owing to their intermediate mass, small hadronic cross section, and precise $v_{2,3}(p_T, \text{cent})$ measurements. Unlike charged-hadron scaling, which averages over species, the kaon reference preserves species identity and enables direct comparison of mass-, baryon-number–, and coupling-dependent responses to a common medium.

The species-resolved scaling functions retain the charged-hadron attenuation parameter $\beta = k_\beta \beta_0$, where $\beta_0$ denotes the attenuation coefficient of the ultra-central reference and $k_\beta$ scales this attenuation for the comparison system or beam energy. This attenuation governs viscous damping and quenching, while two species-dependent response coefficients characterize radial-flow and hadronic effects. The radial-flow-induced blue shift is quantified through $\zeta_{\rm rf}$ via $\zeta_b = (1-\zeta_{\rm rf})^{|n_B|}$, where $n_B$ denotes the baryon number, while the influence of late-stage meson re-scattering is quantified through $\zeta_{\rm hs}$, with $\zeta_m = 1-\zeta_{\rm hs}$. Baryons, through their mass- and baryon-number-dependent blue shifts, provide strong constraints on $\zeta_{\rm rf}$, whereas mesons with larger hadronic cross sections primarily constrain $\zeta_{\rm hs}$. For heavier mesons such as the $\phi$, where $\zeta_{\rm hs}^{(\phi)} \approx 0$, residual deviations from kaon scaling predominantly reflect mass-dependent radial-flow effects rather than hadronic transport. Such species-dependent sensitivity to the hadronic stage is also supported by a recent analysis employing hydrodynamics coupled to a UrQMD hadronic afterburner [40].

Building on the kaon-based reference, the scaling framework employs a minimal set of geometric and response inputs. The initial eccentricities $\varepsilon_n(\text{cent})$ and the transverse size scale $\mathbb{R} \propto \langle N_{\rm ch} \rangle^{1/3}$ provide the system- and centrality-dependent geometric inputs. The response coefficients are constrained simultaneously by intra-harmonic $v_n/\varepsilon_n$ scaling ($n = 2, 3$) and the inter-harmonic $v_3/\varepsilon_3 \to v_2/\varepsilon_2$ mapping over the measured $p_T$ range and across particle species, centralities, collision systems, and beam energies. The inter-harmonic constraint also incorporates the system- and centrality-dependent hierarchy of $\varepsilon_3/\varepsilon_2$ through the geometry-derived input $\gamma^X_{32}$; this hierarchy is generally less sensitive to the initial-state model than the absolute eccentricities. These complementary constraints limit parameter degeneracy because $k_\beta$, $\zeta_{\rm rf}$, and $\zeta_{\rm hs}$ govern distinct and differently evolving attenuation, radial-flow, and hadronic signatures of the scaling, respectively. Consequently, variations in one response coefficient cannot in general be compensated by changes in another without degrading the simultaneous scaling fidelity.

The resulting scaling relations are phenomenological response relations rather than first-principles solutions of hydrodynamic or transport equations. Their structure is motivated by acoustic viscous attenuation, the $\delta f \propto p_T^2$ viscous correction, geometric eccentricity and system-size scaling, and the observed species dependence of radial-flow and hadronic responses. The associated coefficients therefore quantify distinct components of the scaling response; their sensitivity to microscopic transport properties such as $\eta/s$ and $\hat{q}$ provides the physical interpretation, rather than a direct numerical extraction of these quantities. Importantly, the coefficients are not obtained from independent fits to individual $v_n(p_T)$ distributions, but are constrained by the simultaneous scaling requirements over the measured $p_T$ range and across harmonics, particle species, centralities, collision systems, and beam energies.

For mesons, the intra-harmonic $v_2/\varepsilon_2$ scaling relation is

$$\left(\frac{v_2(p_T)}{\varepsilon_2}\right)_{\rm uc} e^{\frac{2\beta_0}{\mathbb{R}_{\rm uc}}(2+\kappa p_T^2)} = e^{\frac{\beta_0}{\mathbb{R}_{\rm uc}}\mathcal{A}_\alpha(p_T)\zeta_M^{(2)}} \times\left(\frac{v_2'(p_T)}{\varepsilon_2'}\right)^{\zeta_m} e^{\frac{2\zeta_m\beta}{\mathbb{R}_{\rm uc}}\left(\frac{\mathbb{R}_{\rm uc}}{\mathbb{R}'}-1\right)(2+\kappa p_T^2)}, \quad (3)$$

where primes denote the comparison system or centrality and $\zeta_M^{(2)} = \zeta_m + \gamma_{32}^X + (1-k_\beta)$ is the corresponding normalization exponent. The geometry-only offset $\gamma_{32}^X \equiv \ln[(\varepsilon_3/\varepsilon_2)_{\rm ref}/(\varepsilon_3/\varepsilon_2)_{\rm sys}]|_X$ is an input determined from the eccentricities of the reference and comparison systems, rather than an independently varied medium-response parameter, where $X$ denotes the applicable centrality regime. The quantity $\gamma_{32}^X$ accounts for inter-system differences in the eccentricity ratio and enters only through the normalization exponents; it does not modify the attenuation or size-dependent terms.

The viscous correction is parameterized as $\delta f = \kappa p_T^2$. The reference-side normalization in Eq. 3 depends on the centrality selection through

$$\mathcal{A}_\alpha(p_T) = \begin{cases} 2, & \alpha = 0, \\ 2\alpha(2+\kappa p_T^2), & \alpha > 0, \end{cases}$$

where $\alpha = 0$, 0.5, and 1 correspond to non-ultra-central, near-ultra-central, and ultra-central selections, respectively. This prescription retains only the $p_T$-independent normalization for non-ultra-central collisions, while near-ultra-central and ultra-central selections retain one-half and the full $p_T$-dependent correction, respectively. The attenuation term proportional to $\beta/\mathbb{R}$ retains its full $(2+\kappa p_T^2)$ dependence for all centrality selections. The baryon relations introduced below retain their explicit $\alpha$ dependence.

The corresponding meson inter-harmonic mapping is

$$\left(\frac{v_2(p_T)}{\varepsilon_2}\right)_{\rm uc} e^{\frac{2\beta_0}{\mathbb{R}_{\rm uc}}(2+\kappa p_T^2)} = e^{\frac{2\beta_0}{\mathbb{R}_{\rm uc}}\zeta_M^{(2\leftarrow3)}} \times\left(\frac{v_3'(p_T)}{\varepsilon_3'}\right)^{\frac{2}{3}\zeta_m} e^{\frac{2\zeta_m\beta}{\mathbb{R}_{\rm uc}}\left(\frac{\mathbb{R}_{\rm uc}}{\mathbb{R}'}-1\right)(3+\kappa p_T^2)}, \quad (4)$$

with $\zeta_M^{(2\leftarrow3)} = 1-\zeta_M^{(2)}$, ensuring a closed, two-constraint normalization scheme. The absence of a $p_T$-dependent prefactor in the reference-side exponential reflects the fact that the change in harmonic order is already accounted for by the $2/3$ exponent.

For baryons, the corresponding intra-harmonic relation retains the explicit $\alpha$ dependence,

$$\left(\frac{v_2(p_T)}{\varepsilon_2}\right)_{\rm uc} e^{\frac{2\beta_0}{\mathbb{R}_{\rm uc}}(2+\kappa p_T^2)} = e^{(1-\alpha)\frac{2\beta_0}{\mathbb{R}_{\rm uc}}(2+\kappa p_T^2)\zeta_B^{(2)}} \times\left(\frac{v_2'(p_T)}{\varepsilon_2'}\right)^{\zeta_b} e^{\frac{2\zeta_b\beta}{\mathbb{R}_{\rm uc}}\left(\frac{\mathbb{R}_{\rm uc}}{\mathbb{R}'}-1\right)(2+\kappa p_T^2)}, \quad (5)$$

where $\zeta_B^{(2)} = -\zeta_b(|n_B|/k_\beta - \gamma_{32}^X)$.

The baryon inter-harmonic mapping is

$$\left(\frac{v_2(p_T)}{\varepsilon_2}\right)_{\rm uc} e^{\frac{2\beta_0}{\mathbb{R}_{\rm uc}}(2+\kappa p_T^2)} = e^{\frac{2\beta_0}{\mathbb{R}_{\rm uc}}\zeta_B^{(2\leftarrow3)}} \times\left(\frac{v_3'(p_T)}{\varepsilon_3'}\right)^{\frac{2}{3}\zeta_b} e^{\frac{2\zeta_b\beta}{\mathbb{R}_{\rm uc}}\left(\frac{\mathbb{R}_{\rm uc}}{\mathbb{R}'}-1\right)(3+\kappa p_T^2)}, \quad (6)$$

with $\zeta_B^{(2\leftarrow3)} = -\zeta_b(2|n_B|/k_\beta + \gamma_{32}^X)$. As in the meson case, the inter-harmonic normalization involves only the harmonic-dependent viscous factor, with no additional $p_T$-dependent prefactor.

For continuity above $p_T^{\rm thresh} \sim 4.5$ GeV/$c$, the $p_T$-dependent viscous correction is held fixed, allowing the same scaling structure to extend continuously from the low- and intermediate-$p_T$ collective regime into the high-$p_T$ quenching-dominated regime while retaining sensitivity to partonic energy-loss effects [36]. Together, Eqs. 3–6 provide complementary intra- and inter-harmonic constraints within a unified species-resolved framework. Their combined scaling fidelity over the measured $p_T$ range and across particle species, centralities, collision systems, and beam energies constrains the geometric, attenuation, radial-flow, and hadronic-response contributions within a common medium-response description.

Beyond encoding the initial-state geometry through $\varepsilon_n$, the species-resolved framework provides additional leverage for constraining intrinsic nuclear deformation. The simultaneous intra-harmonic $v_n/\varepsilon_n$ ($n = 2, 3$) and inter-harmonic $v_3/\varepsilon_3 \to v_2/\varepsilon_2$ scaling requirements make the framework particularly sensitive to changes in the eccentricity spectrum. For near-spherical nuclei, $\varepsilon_3$ is predominantly fluctuation driven, whereas $\varepsilon_2$ can contain a substantial contribution from the average nuclear shape. Intrinsic quadrupole and octupole deformation can modify these contributions differently, changing both the magnitudes and the centrality-dependent hierarchy of $\varepsilon_2$ and $\varepsilon_3$ and, consequently, the inter-harmonic mapping. Centrality regions in which deformation effects are small therefore constrain the common medium response, while deformation-sensitive regions provide additional geometric leverage. This separation allows deterioration or restoration of the simultaneous scaling collapse under variations of the assumed nuclear shape to constrain intrinsic deformation without absorbing its effects into the medium-response coefficients.

To construct and test the species-resolved scaling functions, the analysis employs identified-hadron $v_{2,3}(p_T, \text{cent})$ measurements in Pb+Pb at $\sqrt{s_{NN}} = 2.76$ and 5.02 TeV [43, 44, 45, 46, 41, 47, 42], Xe+Xe at 5.44 TeV [48], Au+Au, Cu+Au, and Cu+Cu at $\sqrt{s_{NN}} = 0.20$ TeV [49, 50, 51, 52], and U+U at $\sqrt{s_{NN}} = 193$ GeV [53], as reported by the ALICE, PHENIX, and STAR collaborations. Initial-state eccentricities $\varepsilon_{2,3}(\text{cent})$ are computed using the MC–quark–Glauber model [35], with deformed Woods–Saxon densities for the collision systems.

For each isotope, the quadrupole and octupole deformation parameters $(\beta_2, \beta_3)$, which characterize the corresponding components of the intrinsic nuclear shape, are varied within controlled ranges about established low-energy nuclear-structure priors [54, 55, 56, 57]. The resulting calculations provide $\varepsilon_{2,3}(\text{cent}; \beta_2, \beta_3)$ with typical uncertainties of approximately 2–3%. For sufficiently small intrinsic deformations, approximately $\beta_2 \lesssim 0.05$–$0.07$ and $\beta_3 \lesssim 0.07$, the deformation-induced changes in $\varepsilon_n$ remain subdominant to event-by-event fluctuations over the relevant centrality range, motivating the $\beta_n \sim 0$ assignments for near-spherical systems in Table 1.

The transverse size scale $\mathbb{R} \propto \langle N_{\rm ch}\rangle^{1/3}$ is obtained from published centrality-dependent charged-particle multiplicity densities $\langle N_{\rm ch}\rangle_{|\eta|\le 0.5}$ [58, 59, 60, 61, 62]. The viscous correction uses $\kappa = 0.17$ $(\text{GeV}/c)^{-2}$, following Ref. [35], and is held fixed across collision systems.

The scaling functions are constructed by applying Eqs. 3–6 to the measured $v_{2,3}(p_T, \text{cent})$ such that the transformed measurements collapse onto a common scaling function $\text{F}_\text{S}(v_n/\varepsilon_n)$, as illustrated in panels (c) of Figs. 1–4. Scaling fidelity is required simultaneously over the measured $p_T$ range and across harmonics, particle species, centralities, collision systems, and beam energies. The intra-harmonic $n = 2$ and $n = 3$ relations and the inter-harmonic $v_3/\varepsilon_3 \to v_2/\varepsilon_2$ mapping therefore provide complementary constraints on the same scaling function rather than independent descriptions of individual data sets.

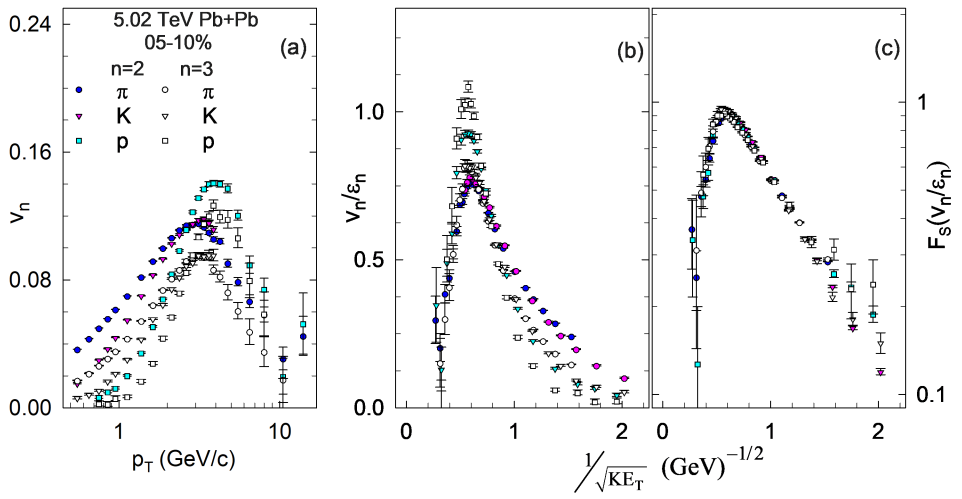


**FIGURE 1:** (Color online) Scaling of $v_2$ and $v_3$ in 5–10% central Pb+Pb collisions at $\sqrt{s_{NN}} = 5.02$ TeV. Panel (a): measured $v_2(p_T)$ and $v_3(p_T)$ for $\pi$, $K$, and $p$, showing clear mass and baryon-number ordering. Panels (b,c): eccentricity-scaled and fully scaled results plotted vs. $1/\sqrt{\mathrm{KE}_T}$. Eccentricity scaling reduces but does not eliminate the species separation (b), while full scaling achieves near-universal behavior across flow-dominated (large $1/\sqrt{\mathrm{KE}_T}$, low $p_T$) and quenching-dominated (small $1/\sqrt{\mathrm{KE}_T}$, high $p_T$) regions. Data from ALICE [41, 42].

Intrinsic deformation provides an additional geometric constraint because variations of $(\beta_2, \beta_3)$ modify $\varepsilon_{2,3}(\mathrm{cent})$ and their hierarchy without changing the measured $v_n$. The preferred deformation parameters are consequently those for which the corresponding eccentricity spectrum gives the highest simultaneous scaling fidelity across the deformation-sensitive and deformation-insensitive selections. In this way, deformation is constrained through the consistency of the full scaling collapse rather than from an isolated $v_n$ magnitude or a single centrality interval.

For cross-species comparisons, the transverse kinetic energy $\mathrm{KE}_T \equiv m_T - m_0$, with $m_T = \sqrt{p_T^2 + m_0^2}$ and $m_0$ the hadron rest mass, is used in place of $p_T$. This representation suppresses trivial kinematic mass differences and provides a common variable for comparing mesons and baryons within the species-resolved scaling framework.

## 3. RESULTS AND DISCUSSION

Figure 1 illustrates the species-resolved scaling procedure for 5–10% central Pb+Pb collisions at $\sqrt{s_{NN}} = 5.02$ TeV. Panel (a) shows the measured $v_2(p_T)$ and $v_3(p_T)$, highlighting the characteristic mass ordering at low $p_T$ and the pronounced species-dependent separation between the two harmonics. Panels (b) and (c) employ $1/\sqrt{\mathrm{KE}_T}$ to delineate the flow- and quenching-dominated regimes [14, 63]. Panel (b) demonstrates that eccentricity and $\mathrm{KE}_T$ scaling, with $\varepsilon_n$ accounting for the initial geometric anisotropy, substantially improve the alignment among species, most clearly for pions and kaons. The remaining blue shift between protons and mesons, together with the residual separation between $v_2$ and $v_3$, provides sensitivity to species-dependent radial flow, hadronic coupling, and the distinct attenuation of the two harmonics.

Panel (c) shows the fully scaled results, for which the identified-hadron measurements collapse onto the common scaling function $\mathrm{F_S}(v_n/\varepsilon_n)$ across both the collective and high-$p_T$ regimes. For this centrality class, the collapse is obtained with $\beta_0 = 0.88$, $k_\beta = 1.0$ (and hence $\beta = \beta_0$), $\zeta_{\mathrm{rf}} = 0.46$, and $\zeta_{\mathrm{hs}} = 0$, while $\gamma_{32}^X = 0$ follows from the reference geometry. The response coefficients are dimensionless and of order unity or smaller, and variations of order $\Delta \sim 0.005$ about their preferred values generally produce discernible changes in the scaling fidelity. Variations of $k_\beta$, $\zeta_{\mathrm{rf}}$, and $\zeta_{\mathrm{hs}}$ generate distinct residual attenuation, species- and baryon-number-dependent, and hadronic-response patterns, respectively, thereby providing an empirical measure of the coefficient resolution and restricting parameter interchangeability. These values are summarized in Table 1.

The resulting response pattern is consistent with anisotropies dominated by QGP-driven dynamics, including viscous attenuation, partonic energy loss, and strong radial flow, with negligible influence from late-stage hadronic re-scattering indicated by $\zeta_{\mathrm{hs}} = 0$ for this centrality class. The simultaneous collapse of $v_2$ and $v_3$ for mesons and baryons with different masses, baryon numbers, and hadronic couplings provides a nontrivial test of the species-resolved framework. In particular, the same response description accommodates the measured anisotropies over the full $p_T$ range without assigning independent response parameters to individual $v_n(p_T)$ distributions.

Figure 2 extends this test to $v_2(p_T)$ in 30–40% central Pb+Pb collisions at $\sqrt{s_{NN}} = 5.02$ TeV, including mesons ($\pi$, $K$, $K^0_S$, $\phi$) and baryons ($p$, $\Lambda^0$, $\Xi^-$, $^3$He). Panel (a) shows the measured $v_2(p_T)$ and its characteristic mass and baryon-number ordering. Panel (b) demonstrates substantial inter-species convergence after eccentricity and $\mathrm{KE}_T$ scaling. Pions and kaons approach a common meson curve, while the $\phi$ retains a modest offset consistent with its small hadronic cross section and mass-dependent radial-flow response. Baryons with $|n_B| = 1$ follow a distinct blue-shifted trend, while the larger shift of $^3$He ($|n_B| = 3$) provides additional leverage on the baryon-number dependence of the radial-flow response. The residual species separations therefore provide complementary constraints on the transformations required to obtain the common scaling function.

Panel (c) shows the fully scaled results, for which the identified species collapse onto $\mathrm{F_S}(v_n/\varepsilon_n)$. Relative to the 5–10% selection shown in Fig. 1, the smaller $\zeta_{\mathrm{rf}}$ reflects the weaker radial-flow response in the more peripheral 30–40% selection, whereas $k_\beta$ and $\zeta_{\mathrm{hs}}$ remain unchanged. The simultaneous alignment of the $|n_B| = 1$ baryons and $^3$He provides a particularly stringent test of

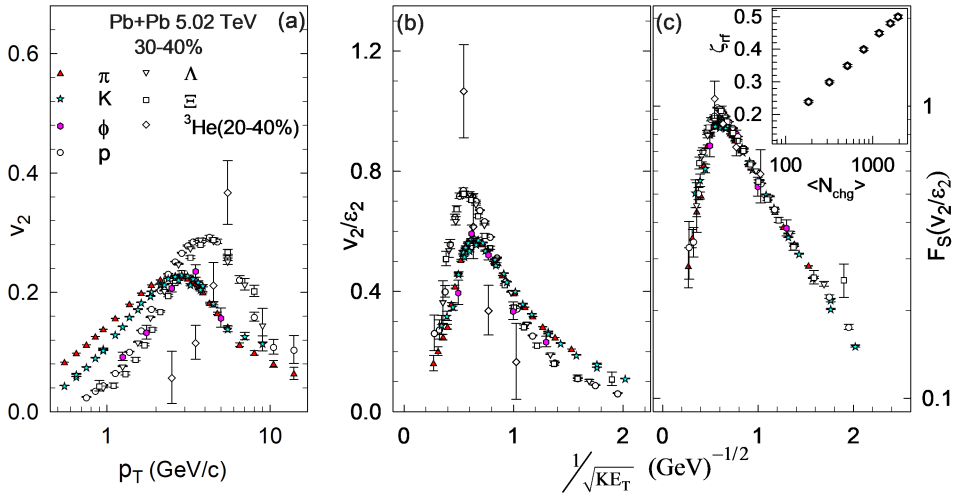


**FIGURE 2:** (Color online) Scaling of $v_2$ in 30–40% central Pb+Pb collisions at $\sqrt{s_{NN}} = 5.02$ TeV. Panel (a): measured $v_2(p_T)$ for mesons ($\pi$, $K$, $K^0_S$, $\phi$) and baryons ($p$, $\Lambda^0$, $\Xi$, $^3$He). Panels (b,c): eccentricity-scaled and fully scaled results plotted vs. $1/\sqrt{\mathrm{KE}_T}$. Inset (c): centrality dependence of $\zeta_{\mathrm{rf}}$ as a function of $\langle N_{\mathrm{ch}}\rangle_{|\eta|\leq 0.5}$. Data from ALICE [41, 47, 42].

$\zeta_b = (1-\zeta_{\mathrm{rf}})^{|n_B|}$: the same $\zeta_{\mathrm{rf}}$ must account for species with different baryon number rather than being adjusted independently for each species. The reduced baryon blue shift relative to Fig. 1 thus tracks the centrality evolution of the radial-flow response while preserving the common attenuation and geometric constraints.

Scaling collapse is obtained for 5.02 TeV Pb+Pb collisions over the analyzed 0–1% to 50–60% centrality range. The corresponding $\zeta_{\mathrm{rf}}$ values, shown in the inset of Fig. 2 as a function of $\langle N_{\mathrm{ch}}\rangle_{|\eta|\leq 0.5}$, increase approximately logarithmically with multiplicity. This behavior is consistent with the expected strengthening of radial flow as the density and collective expansion increase and, through the connection between radial acceleration and the medium pressure, retains sensitivity to the equation of state.

The extracted centrality trends also provide an empirical test of the separation among the response coefficients. While $\zeta_{\mathrm{rf}}$ evolves systematically with centrality, $k_\beta$ and $\zeta_{\mathrm{hs}}$ remain comparatively stable in Pb+Pb at this beam energy. These differently evolving radial-flow, attenuation, and hadronic-response signatures reinforce the simultaneous scaling constraints and limit the extent to which changes in one response coefficient can be compensated by variations in another without degrading the scaling fidelity.

Robust species-resolved scaling functions, closely matching those obtained for 5.02 TeV Pb+Pb, are observed across a broad range of collision systems and beam energies, including Xe+Xe at 5.44 TeV, Pb+Pb at 2.76 TeV, Au+Au, Cu+Au, and Cu+Cu at $\sqrt{s_{NN}} = 200$ GeV, and U+U at $\sqrt{s_{NN}} = 193$ GeV. For the systems and centralities analyzed, the measured $v_{2,3}(p_T, \mathrm{cent})$ are brought onto the common scaling function once the corresponding geometric and species-response inputs are applied, extending the test of the framework well beyond the 5.02 TeV Pb+Pb reference system. Figures 3 and 4 present representative examples at the lower LHC energy and top RHIC energy, respectively.

Table 1 summarizes representative response parameters associated with the scaling collapse for the systems and centralities shown, together with the corresponding quadrupole deformation parameter $\beta_2$. The response coefficients $k_\beta$, $\zeta_{\mathrm{rf}}$, and $\zeta_{\mathrm{hs}}$ are constrained by the simultaneous scaling requirements, whereas the eccentricities and the geometry-derived normalization $\gamma^X_{32}$ enter separately as inputs to the analysis. Although the table is not exhaustive in centrality coverage, it illustrates the systematic changes of the response coefficients with beam energy, collision system, and centrality. The more complete centrality dependence of $\zeta_{\mathrm{rf}}$ is shown as a function of multiplicity in the insets of Figs. 2–4.

| System | $\sqrt{s_{NN}}$ (TeV) | cent (%) | $k_\beta$ | $\zeta_{\mathrm{rf}}$ | $\zeta_{\mathrm{hs}}$ | $\beta_2$ |
|---|---|---|---|---|---|---|
| Pb+Pb | 5.02 | 5–10 | 1.00 | 0.46 | 0.00 | $\sim 0$ |
| Pb+Pb | 5.02 | 30–40 | 1.00 | 0.35 | 0.00 | $\sim 0$ |
| Pb+Pb | 2.76 | 20–30 | 0.95 | 0.37 | 0.00 | $\sim 0$ |
| Xe+Xe | 5.44 | 0–5 | 1.02 | 0.43 | 0.00 | 0.18 |
| Au+Au | 0.20 | 0–30 | 0.63 | 0.29 | 0.08 | $\sim 0$ |
| Cu+Au | 0.20 | 20–30 | 0.63 | 0.22 | 0.08 | $\sim 0$ |
| Cu+Cu | 0.20 | 20–30 | 0.63 | 0.20 | 0.11 | $\sim 0$ |
| U+U | 0.193 | 0–10 | 0.63 | 0.28 | 0.08 | 0.20 |

**TABLE 1:** Representative response parameters associated with species-resolved scaling for selected collision systems and centralities, together with the quadrupole deformation parameter $\beta_2$. The response coefficients $k_\beta$, $\zeta_{\mathrm{rf}}$, and $\zeta_{\mathrm{hs}}$ are constrained by the simultaneous scaling requirements, while the eccentricities and the geometry-derived normalization $\gamma^X_{32}$ enter separately as inputs to the scaling analysis. Representative scaling collapses are shown in Figs. 1–4.

Figure 3 shows the species-resolved scaling procedure for 20–30% central Pb+Pb collisions at $\sqrt{s_{NN}} = 2.76$ TeV, enabling a direct comparison with the 5.02 TeV results in Fig. 2. As at the higher energy, eccentricity and $\mathrm{KE}_T$ scaling substantially reduce the species separation, and the full transformation collapses the identified-particle $v_2(p_T)$ onto the common scaling function $\mathrm{F_S}(v_n/\varepsilon_n)$. The modest reduction of $k_\beta$ relative to the 5.02 TeV reference indicates a weak beam-energy dependence of the attenuation response within the LHC energy range. Notably, $\zeta_{\mathrm{rf}}$ is comparable to that for 30–40% central Pb+Pb at 5.02 TeV despite the different beam energy and multiplic-

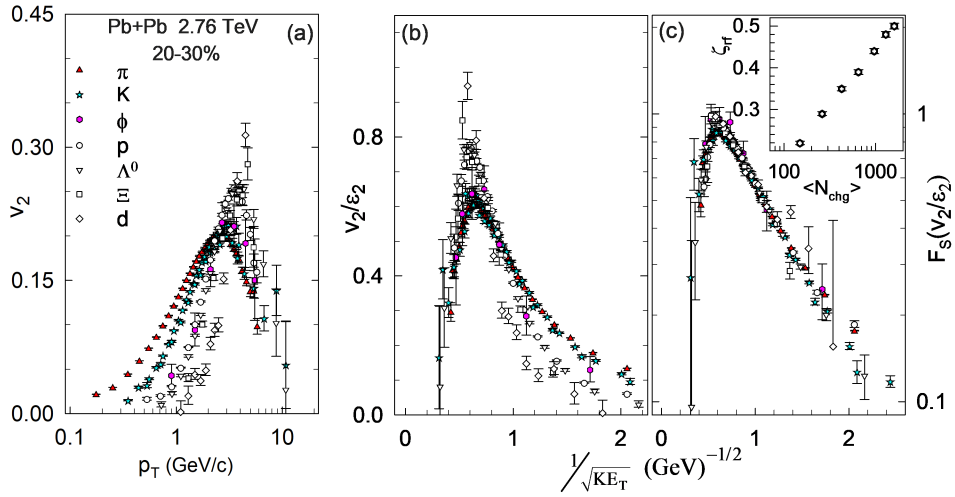


**FIGURE 3:** (Color online) Scaling of $v_2$ in 20–30% central Pb+Pb collisions at $\sqrt{s_{NN}} = 2.76$ TeV. Panel (a): measured $v_2(p_T)$. Panels (b,c): eccentricity-scaled and fully scaled results plotted vs. $1/\sqrt{\mathrm{KE}_T}$, following Fig. 2. Inset (c): centrality dependence of $\zeta_{\mathrm{rf}}$ as a function of $\langle N_{\mathrm{ch}}\rangle_{|\eta|\leq 0.5}$. Data from ALICE [43, 44, 45, 46].

ity. Thus, although $\zeta_{\mathrm{rf}}$ evolves strongly with multiplicity within a fixed beam energy, the cross-energy comparison indicates that multiplicity alone does not determine the radial-flow response.

Figure 4 presents the corresponding species-resolved scaling analysis for 0–30% central Au+Au collisions at $\sqrt{s_{NN}} = 200$ GeV, representative of top RHIC energy. Despite the substantially lower beam energy, robust scaling collapse is again obtained across identified mesons and baryons after accounting for the corresponding geometric, size, and species-response effects. Compared with the LHC examples, panel (b) exhibits a reduced baryon–meson blue shift, reflected in the smaller $\zeta_{\mathrm{rf}}$. In addition, the finite $\zeta_{\mathrm{hs}}$ indicates a larger relative influence of late-stage hadronic re-scattering than in the LHC systems shown. The persistence of the collapse across the measured $p_T$ range demonstrates that the same scaling structure remains applicable as the relative contributions from radial flow, attenuation, and hadronic interactions change substantially with beam energy.

For near-ultra-central (0–5%) collisions, the eccentricity ratio $\varepsilon_3/\varepsilon_2$ is approximately system independent for near-spherical nuclei, yielding $\gamma_{32}^X \simeq 0$. Intrinsic deformation modifies this hierarchy. In systems such as Xe+Xe and U+U, quadrupole deformation enhances $\varepsilon_2$ in ultra-central and near-ultra-central events and consequently changes $\varepsilon_3/\varepsilon_2$, producing a nonzero $\gamma_{32}^X$. Toward mid-central collisions, the ratio approaches a more fluctuation-dominated, system-dependent trend with reduced sensitivity to intrinsic deformation. The resulting ordering of $\varepsilon_3/\varepsilon_2$ across systems determines the sign and relative magnitude of the geometry-derived $\gamma_{32}^X$ values used in the scaling analysis.

The preferred quadrupole deformations are determined by varying the nuclear shape inputs and requiring simultaneous scaling fidelity across the deformation-sensitive and deformation-insensitive selections. This procedure gives preferred values of $\beta_2 \approx 0.18$ for Xe and $\beta_2 \approx 0.20$ for U. The sensitivity to $\beta_2$ is governed by both the response of the calculated eccentricities to variations of the nuclear deformation and the corresponding change in the global scaling fidelity. Variations of $\Delta\beta_2 \sim 0.01$ produce only small changes in the relevant eccentricities, providing an estimate of the deformation resolution of the combined eccentricity–scaling procedure. The Xe value is consistent with that obtained previously from charged-hadron scaling [36], while the preferred U value is also consistent with the independent deformation constraints obtained from the STAR flow analysis [64].

The system dependence provides an additional internal consistency check. The same scaling procedure requires little to no intrinsic quadrupole deformation for Pb, Au, and Cu, while finite deformation is favored for Xe and U. The geometrically asymmetric Cu+Au system provides a particularly useful control: although the collision asymmetry modifies the eccentricity hierarchy, this effect is incorporated through the calculated $\varepsilon_n$ and does not require a corresponding intrinsic-deformation contribution from the Cu or Au nuclei. These systematics support the interpretation that the deformation sensitivity reflects intrinsic nuclear structure rather than collision-system asymmetry or a generic adjustment of the scaling collapse.

Taken together, the cross-system and cross-energy results extend the coefficient-separation test established from the Pb+Pb centrality dependence. The three response coefficients exhibit distinct and differently evolving systematics: $k_\beta$ changes primarily with beam energy and attenuation conditions and is comparatively stable with centrality in the large systems studied; $\zeta_{\mathrm{rf}}$ evolves strongly with centrality and multiplicity and also retains beam-energy and system dependence; and $\zeta_{\mathrm{hs}}$ is negligible for the LHC cases shown but finite for the RHIC systems. These different trends, combined with the simultaneous intra-harmonic, inter-harmonic, species, centrality, system-size, and beam-energy scaling requirements, substantially restrict the extent to which one response coefficient can compensate for another while preserving the global scaling fidelity.

State-of-the-art hydrodynamic calculations, such as IP-Glasma + MUSIC [65, 33], provide detailed dynamical descriptions of anisotropic flow in the low-$p_T$ collective regime. In such calculations, however, radial flow, viscous attenuation, and late-stage hadronic effects emerge jointly from the dynamical evolution, so their individual experimental trends generally require dedicated model comparisons or controlled variations. The present species-resolved scaling framework provides a complementary, data-driven perspective by charting the corresponding response coefficients directly across centrality, collision system, and beam energy. Its common response structure also extends continuously from the collective regime into the high-$p_T$ region, where partonic energy loss becomes increasingly important.

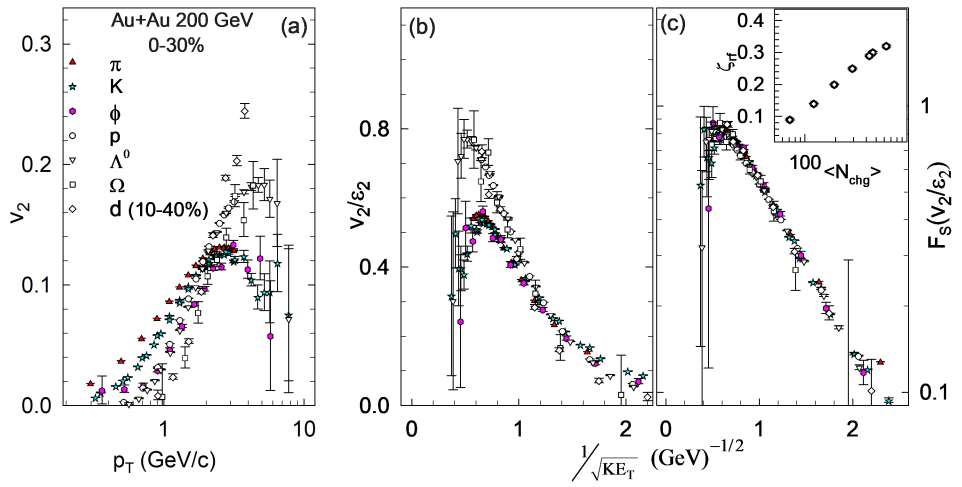


**FIGURE 4:** (Color online) Scaling of $v_2$ in 0–30% central Au+Au collisions at $\sqrt{s_{NN}} = 0.20$ TeV. Panel (a): measured $v_2(p_T)$. Panels (b,c): eccentricity-scaled and fully scaled results plotted vs. $1/\sqrt{\mathrm{KE}_T}$. Full scaling in panel (c) achieves near-universal behavior across mesons ($\pi$, $K$, $K^0_S$, $\phi$) and baryons ($p$, $\Lambda^0$, $\Omega$, $d$), spanning the transition from collective to quenching-dominated regimes. Inset (c): centrality dependence of $\zeta_{\mathrm{rf}}$ as a function of $\langle N_{\mathrm{ch}}\rangle_{|\eta|\leq 0.5}$. Data from PHENIX and STAR [49, 50, 52].

The resulting systematics support a unified, data-driven description of azimuthal anisotropy from low-$p_T$ collective behavior into the high-$p_T$ quenching-dominated regime. Within this framework, $k_\beta$ provides sensitivity to viscous attenuation and partonic energy loss, while $\zeta_{\mathrm{rf}}$ and $\zeta_{\mathrm{hs}}$ quantify the radial-flow and hadronic responses, respectively. Their combined behavior therefore provides complementary constraints on QGP transport, collective expansion, and late-stage hadronic dynamics across collision systems and beam energies.

## 4. SUMMARY AND CONCLUSIONS

This study presents a species-resolved scaling framework for azimuthal anisotropy in identified mesons and baryons over a broad $p_T$ range and across particle species, centralities, collision systems, and beam energies. The simultaneous analysis of $v_2(p_T, \mathrm{cent})$ and $v_3(p_T, \mathrm{cent})$, through both intra-harmonic scaling and inter-harmonic mapping, separates the geometric inputs from response coefficients associated with attenuation, radial flow, and hadronic re-scattering, while incorporating the baryon-number dependence of the radial-flow response. The framework extends continuously from the low-$p_T$ collective regime into the high-$p_T$ region where partonic energy loss becomes increasingly important. The constrained response coefficients exhibit distinct and systematic trends: $k_\beta$ varies primarily with beam energy and attenuation conditions and remains comparatively stable with centrality in the large systems studied; $\zeta_{\mathrm{rf}}$ shows a pronounced dependence on centrality and multiplicity, together with additional system and beam-energy dependence; and $\zeta_{\mathrm{hs}}$ is negligible for the LHC cases studied and finite for the RHIC systems. These differently evolving signatures, together with the simultaneous constraints from harmonic order, particle species, baryon number, centrality, system size, and beam energy, substantially restrict interchangeability among the response coefficients. The resulting systematics provide complementary sensitivity to viscous attenuation and partonic energy loss through $k_\beta$, while $\zeta_{\mathrm{rf}}$ and $\zeta_{\mathrm{hs}}$ quantify the radial-flow and hadronic responses, respectively. The evolution of $\zeta_{\mathrm{rf}}$ also provides sensitivity to pressure-driven collective expansion and hence to the equation of state, while the geometry-sensitive inter-harmonic constraints provide sensitivity to intrinsic nuclear deformation, with preferred quadrupole deformations of $\beta_2 \approx 0.18$ for Xe and $\beta_2 \approx 0.20$ for U. This deformation sensitivity is reinforced by the system dependence: the scaling requires little to no intrinsic quadrupole deformation for Pb, Au, and Cu, while the geometrically asymmetric Cu+Au system modifies the eccentricity hierarchy without requiring a corresponding intrinsic-deformation contribution. The persistence of high-fidelity scaling over the analyzed $p_T$ range and across particle species, centralities, collision systems, and beam energies demonstrates the broad applicability of the framework and establishes species-resolved anisotropy scaling as a quantitative, complementary tool for constraining QGP transport, collective expansion, late-stage hadronic dynamics, and initial-state nuclear structure.

## References


[1] E. V. Shuryak, Phys. Rept. **115**, 151 (1984).

[2] S. A. Bass, M. Gyulassy, H. Stoecker, and W. Greiner, J. Phys. G **25**, R1 (1999), arXiv:hep-ph/9810281 .

[3] H. Satz, Rept. Prog. Phys. **63**, 1511 (2000), arXiv:hep-ph/0007069 .

[4] A. Bilandzic, R. Snellings, and S. Voloshin, Phys. Rev. **C83**, 044913 (2011), arXiv:1010.0233 [nucl-ex] .

[5] M. Luzum, J. Phys. **G38**, 124026 (2011), arXiv:1107.0592 [nucl-th] .

[6] D. Teaney and L. Yan, Phys. Rev. **C86**, 044908 (2012), arXiv:1206.1905 [nucl-th] .

[7] C. Adler *et al.* (STAR), Phys. Rev. **C66**, 034904 (2002), arXiv:nucl-ex/0206001 [nucl-ex] .

[8] S. A. Voloshin, A. M. Poskanzer, and R. Snellings, Landolt-Bornstein **23**, 293 (2010), arXiv:0809.2949 [nucl-ex] .

[9] H. Song, S. A. Bass, U. Heinz, T. Hirano, and C. Shen, Phys. Rev. Lett. **106**, 192301 (2011), [Erratum: Phys. Rev. Lett.109,139904(2012)], arXiv:1011.2783 [nucl-th] .

[10] B. Alver *et al.* (PHOBOS), Phys. Rev. **C77**, 014906 (2008), arXiv:0711.3724 [nucl-ex] .

[11] B. Alver *et al.* (PHOBOS), Phys. Rev. **C81**, 034915 (2010), arXiv:1002.0534 [nucl-ex] .

[12] J.-Y. Ollitrault, A. M. Poskanzer, and S. A. Voloshin, Phys. Rev. C **80**, 014904 (2009), arXiv:0904.2315 [nucl-ex] .

[13] K. Dusling, G. D. Moore, and D. Teaney, Phys.Rev. **C81**, 034907 (2010), arXiv:0909.0754 [nucl-th] .

[14] R. A. Lacey, A. Taranenko, R. Wei, N. Ajitanand, J. Alexander, *et al.*, Phys.Rev. **C82**, 034910 (2010), arXiv:1005.4979 [nucl-ex] .

[15] C. Shen, U. Heinz, P. Huovinen, and H. Song, Phys. Rev. C **84**, 044903 (2011), arXiv:1105.3226 [nucl-th] .

[16] H. Niemi, G. S. Denicol, H. Holopainen, and P. Huovinen, Phys. Rev. **C87**, 054901 (2013), arXiv:1212.1008 [nucl-th] .

[17] J. Fu, Phys. Rev. **C92**, 024904 (2015).

[18] C. Andrés, J. Dias de Deus, A. Moscoso, C. Pajares, and C. A. Salgado, EPJ Web Conf. **90**, 08003 (2015).

[19] M. Abdallah *et al.* (STAR), Phys. Rev. Lett. **129**, 252301 (2022), arXiv:2201.10365 [nucl-ex] .

[20] J. Adam *et al.* (STAR), Phys. Lett. **B783**, 459 (2018), arXiv:1803.03876 [nucl-ex] .

[21] J. Adam *et al.* (ALICE), Phys. Rev. Lett. **117**, 182301 (2016), arXiv:1604.07663 [nucl-ex] .

[22] Z. Qiu and U. W. Heinz, Phys. Rev. C **84**, 024911 (2011), arXiv:1104.0650 [nucl-th] .

[23] A. Adare *et al.* (PHENIX), Phys. Rev. Lett. **107**, 252301 (2011), arXiv:1105.3928 [nucl-ex] .

[24] N. Magdy (STAR), *Proceedings, 27th International Conference on Ultrarelativistic Nucleus-Nucleus Collisions (Quark Matter 2018): Venice, Italy, May 14-19, 2018*, Nucl. Phys. **A982**, 255 (2019), arXiv:1807.07638 [nucl-ex] .

[25] L. Adamczyk *et al.* (STAR), Phys. Rev. C **94**, 034908 (2016), arXiv:1601.07052 [nucl-ex] .

[26] L. Adamczyk *et al.* (STAR), Phys. Rev. C **93**, 014907 (2016), arXiv:1509.08397 [nucl-ex] .

[27] L. Adamczyk *et al.* (STAR), Phys. Rev. Lett. **115**, 222301 (2015).

[28] L. Adamczyk *et al.* (STAR), Phys. Rev. Lett. **116**, 112302 (2016), arXiv:1601.01999 [nucl-ex] .

[29] J. Adam *et al.* (STAR), Phys. Rev. Lett. **122**, 172301 (2019), arXiv:1901.08155 [nucl-ex] .

[30] F. G. Gardim, J. Noronha-Hostler, M. Luzum, and F. Grassi, Phys. Rev. **C91**, 034902 (2015), arXiv:1411.2574 [nucl-th] .

[31] H. Holopainen, H. Niemi, and K. J. Eskola, Phys. Rev. **C83**, 034901 (2011), arXiv:1007.0368 [hep-ph] .

[32] G.-Y. Qin, H. Petersen, S. A. Bass, and B. Muller, Phys. Rev. C **82**, 064903 (2010), arXiv:1009.1847 [nucl-th] .

[33] C. Gale, S. Jeon, B. Schenke, P. Tribedy, and R. Venugopalan, Phys. Rev. Lett. **110**, 012302 (2013), arXiv:1209.6330 [nucl-th] .

[34] K. M. Burke *et al.* (JET), Phys. Rev. C **90**, 014909 (2014), arXiv:1312.5003 [nucl-th] .

[35] P. Liu and R. A. Lacey, Phys. Rev. C **98**, 021902 (2018), arXiv:1802.06595 [nucl-ex] .

[36] R. A. Lacey, Phys. Rev. C **110**, L031901 (2024), arXiv:2402.09389 [nucl-ex] .

[37] T. Parida, R. Samanta, and J.-Y. Ollitrault, Phys. Lett. B **857**, 138985 (2024), arXiv:2407.17313 [nucl-th] .

[38] B. Schenke, C. Shen, and D. Teaney, Phys. Rev. C **102**, 034905 (2020), arXiv:2004.00690 [nucl-th] .

[39] R. A. Lacey, Phys. Lett. B **876**, 140357 (2026), arXiv:2410.22688 [nucl-ex] .

[40] R. Lacey, (2026), arXiv:2604.27254 [nucl-th] .

[41] Y. Zhu (ALICE), PoS **ICHEP2018**, 441 (2019).

[42] S. Acharya *et al.* (ALICE), JHEP **05**, 243 (2023), arXiv:2206.04587 [nucl-ex] .

[43] B. B. Abelev *et al.* (ALICE), JHEP **06**, 190 (2015), arXiv:1405.4632 [nucl-ex] .

[44] J. Adam *et al.* (ALICE), JHEP **09**, 164 (2016), arXiv:1606.06057 [nucl-ex] .

[45] S. Acharya *et al.* (ALICE), Eur. Phys. J. C **77**, 658 (2017), arXiv:1707.07304 [nucl-ex] .

[46] S. Acharya *et al.* (ALICE), Phys. Lett. B **784**, 82 (2018), arXiv:1805.01832 [nucl-ex] .

[47] S. Acharya *et al.* (ALICE), Phys. Rev. C **102**, 055203 (2020), arXiv:2005.14639 [nucl-ex] .

[48] S. Acharya *et al.* (ALICE), JHEP **10**, 152 (2021), arXiv:2107.10592 [nucl-ex] .

[49] A. Adare *et al.* (PHENIX), Phys. Rev. C **93**, 051902 (2016), arXiv:1412.1038 [nucl-ex] .

[50] L. Adamczyk *et al.* (STAR), Phys. Rev. Lett. **116**, 062301 (2016), arXiv:1507.05247 [nucl-ex] .

[51] L. Adamczyk *et al.* (STAR), Phys. Rev. C **98**, 014915 (2018), arXiv:1712.01332 [nucl-ex] .

[52] M. Abdallah *et al.* (STAR), Phys. Rev. C **105**, 064911 (2022), arXiv:2203.07204 [nucl-ex] .

[53] M. Abdallah *et al.* (STAR), Phys. Rev. C **103**, 064907 (2021), arXiv:2103.09451 [nucl-ex] .

[54] P. Möller, R. Bengtsson, B. G. Carlsson, P. Olivius, T. Ichikawa, H. Sagawa, and A. Iwamoto, Atom. Data Nucl. Data Tabl. **94**, 758 (2008).

[55] P. Möller, A. J. Sierk, T. Ichikawa, and H. Sagawa, Atom. Data Nucl. Data Tabl. **109-110**, 1 (2016), arXiv:1508.06294 [nucl-th] .

[56] B. Pritychenko, M. Birch, B. Singh, and M. Horoi, Atom. Data Nucl. Data Tabl. **107**, 1 (2016), [Erratum: Atom.Data Nucl.Data Tabl. 114, 371–374 (2017)], arXiv:1312.5975 [nucl-th] .

[57] P. A. Butler and W. Nazarewicz, Rev. Mod. Phys. **68**, 349 (1996).

[58] K. Aamodt *et al.* (ALICE), Phys. Rev. Lett. **106**, 032301 (2011), arXiv:1012.1657 [nucl-ex] .

[59] J. Adam *et al.* (ALICE), Phys. Rev. Lett. **116**, 222302 (2016), arXiv:1512.06104 [nucl-ex] .

[60] S. Acharya *et al.* (ALICE), Phys. Lett. B **790**, 35 (2019), arXiv:1805.04432 [nucl-ex] .

[61] A. M. Sirunyan *et al.* (CMS), Phys. Lett. B **799**, 135049 (2019), arXiv:1902.03603 [hep-ex] .

[62] R. A. Lacey, P. Liu, N. Magdy, M. Csanád, B. Schweid, N. N. Ajitanand, J. Alexander, and R. Pak, Universe **4**, 22 (2018), arXiv:1601.06001 [nucl-ex] .

[63] Y. L. Dokshitzer and D. E. Kharzeev, Phys. Lett. B **519**, 199 (2001), arXiv:hep-ph/0106202 .

[64] M. I. Abdulhamid *et al.* (STAR), Nature **635**, 67 (2024), arXiv:2401.06625 [nucl-ex] .

[65] B. Schenke, S. Jeon, and C. Gale, Phys. Rev. Lett. **106**, 042301 (2011), arXiv:1009.3244 [hep-ph] .